A Journal of Macroecology

Global Ecology and Biogeography

RESEARCH PAPER

Application of the metabolic scaling theory and water–energy balance equation to model large-scale patterns of maximum forest canopy height

Sungho Choi[1]*, Christopher P. Kempes[2], Taejin Park[1], Sangram Ganguly[3], Weile Wang[4], Liang Xu[5], Saikat Basu[6], Jennifer L. Dungan[7], Marc Simard[8], Sassan S. Saatchi[8], Shilong Piao[9], Xiliang Ni[10], Yuli Shi[11], Chunxiang Cao[10], Ramakrishna R. Nemani[12], Yuri Knyazikhin[1] and Ranga B. Myneni[1]

[1]*Department of Earth and Environment, Boston University, Boston, MA 02215, USA,* [2]*Control and Dynamical Systems, California Institute of Technology, Pasadena, CA 91125, USA/The Santa Fe Institute, Santa Fe, NM 87501, USA,* [3]*Bay Area Environmental Research Institute (BAERI) and NASA Ames Research Center, Moffett Field, CA 94035, USA,* [4]*Division of Science and Environmental Policy, California State University Monterey Bay, Seaside, CA 93955/ Biospheric Science Branch, NASA Ames Research Center, Moffett Field, CA 94035, USA,* [5]*Institute of the Environment and Sustainability, University of California, Los Angeles, CA 90095, USA,* [6]*Department of Computer Science, Louisiana State University, Baton Rouge, LA 70803, USA,* [7]*Earth Science Division, NASA Ames Research Center, Moffett Field, CA 94035, USA,* [8]*Jet Propulsion Laboratory, California Institute of Technology, Pasadena, CA 91109, USA,* [9]*College of Urban and Environmental Sciences and Sino-French Institute for Earth System Science, Peking University, Beijing, 100871, China,* [10]*State Key Laboratory of Remote Sensing Sciences, Institute of Remote Sensing Applications, Chinese Academy of Sciences, Beijing, 100101, China,* [11]*School of Remote Sensing, Nanjing University of Information Science and Technology, Nanjing, 210044, China,* [12]*NASA Advanced Supercomputing Division, NASA Ames Research Center, Moffett Field, CA 94035, USA*

*Correspondence: Sungho Choi, Department of Earth and Environment, Boston University, Boston, MA 02215, USA.
E-mail: schoi@bu.edu

ABSTRACT

Aim Forest height, an important biophysical property, underlies the distribution of carbon stocks across scales. Because *in situ* observations are labour intensive and thus impractical for large-scale mapping and monitoring of forest heights, most previous studies adopted statistical approaches to help alleviate measured data discontinuity in space and time. Here, we document an improved modelling approach which links metabolic scaling theory and the water–energy balance equation with actual observations in order to produce large-scale patterns of forest heights.

Methods Our model, called allometric scaling and resource limitations (ASRL), accounts for the size-dependent metabolism of trees whose maximum growth is constrained by local resource availability. Geospatial predictors used in the model are altitude and monthly precipitation, solar radiation, temperature, vapour pressure and wind speed. Disturbance history (i.e. stand age) is also incorporated to estimate contemporary forest heights.

Results This study provides a baseline map (*c.* 2005; 1-km^2 grids) of forest heights over the contiguous United States. The Pacific Northwest/California is predicted as the most favourable region for hosting large trees (*c.* 100 m) because of sufficient annual precipitation (> 1400 mm), moderate solar radiation (*c.* 330 W m^{-2}) and temperature (*c.* 14 °C). Our results at sub-regional level are generally in good and statistically significant (P-value < 0.001) agreement with independent reference datasets: field measurements [mean absolute error (MAE) = 4.0 m], airborne/spaceborne lidar (MAE = 7.0 m) and an existing global forest height product (MAE = 4.9 m). Model uncertainties at county level are also discussed in this study.

Main conclusions We improved the metabolic scaling theory to address variations in vertical forest structure due to ecoregion and plant functional type. A clear mechanistic understanding embedded within the model allowed synergistic combinations between actual observations and multiple geopredictors in forest height mapping. This approach shows potential for prognostic applications, unlike previous statistical approaches.

Keywords

Carbon monitoring, disturbance history, geospatial predictors, large-scale modelling, maximum forest height, mechanistic understanding, metabolic scaling theory, prognostic applications, water–energy balance.

DOI: 10.1111/geb.12503
http://wileyonlinelibrary.com/journal/geb

INTRODUCTION

Forest height is used in the quantification of forest carbon across local, regional and global scales (Pan *et al.*, 2013). Systematic field sampling might be the most accurate method for recurrent monitoring of forest heights. However, this labour-intensive method is impractical for large-scale carbon accounting owing to data discontinuity in space and time. Remote sensing techniques may alleviate the limitation of field measurements (Goetz *et al.*, 2009). Airborne lidar and stereo-photogrammetry data can capture vertical forest structure with local-to-regional coverage, but the application to continental and global mapping is data-limited and expensive (Goetz & Dubayah, 2011). While the spaceborne lidar (Geoscience Laser Altimeter System, GLAS) aboard the Ice, Cloud, and Land Elevation Satellite (ICESat) has provided global-scale altimetry information (Zwally *et al.*, 2012), these data still have an insufficient sampling density for the complete monitoring of equatorial and mid-latitude forests (Tang *et al.*, 2014).

Recent modelling approaches have combined the sparse observations with multiple geospatial predictors, which are already available at large scales, to generate continuous patterns of forest height (Lefsky, 2010; Simard *et al.*, 2011; Hansen *et al.*, 2014). For instance, climatic variables are good candidates for useful predictors based on an assumption that climate regulates overall plant growth (Nemani *et al.*, 2003; Wu *et al.*, 2011; Peng *et al.*, 2013). Such models, including spatial statistics and machine learning algorithms, are highly predictive and enable large-scale monitoring of forest carbon. However, physical and biological principles underlying forest growth are often neglected in those approaches, and this limitation may lead to non-mechanistic shifts in the modelled outputs that are easily affected by the quality and quantity of training data (Stojanova *et al.*, 2010). These approaches are generally unsuitable for recurring assessments of biomass change or prognostic applications because the correlations established in the models are difficult to reproduce for different study areas or times. Ideally, a model grounded in explicit mechanistic principles is more prognostic and provides a better understanding of forest dynamics or processes governing changes in forest carbon pools and their flux.

The present study applies and updates a biophysical approach (Kempes *et al.*, 2011), which can be combined with actual observations, in order to produce large-scale and continuous patterns of forest canopy heights. Our model, called allometric scaling and resource limitations (ASRL), integrates metabolic scaling theory for plants (MST; West *et al.*, 1997) and the water–energy balance equation [Penman–Monteith (PM); Monteith & Unsworth, 2013]. The biophysical principles embedded within the model provide a generalized mechanistic understanding of relationships between vertical forest structure and geospatial predictors, including topography and climatic variables.

The MST hypothesizes that plant metabolic rate B (respiration, photosynthesis or xylem flow) scales with the geometry of the vascular network (e.g. xylem) and consequently dictates the size of the whole plant (volume V or mass M) as: $B \propto V^{\theta} \propto M^{\theta}$ (West *et al.*, 1999). The exponent θ is close to 3/4, consistent with the three-quarter power rule for living organisms (Kleiber, 1947), although other exponent values could be incorporated. The theory supposes an idealized tree with a constant tissue density ($M = \rho V = \rho\pi r_{\text{stem}}^2 h$ with density ρ, stem radius r_{stem} and tree height h) where the xylem flow rate Q_0 represents the minimum required (i.e. life sustaining) water circulation. The theoretical Q_0 is interrelated with r_{stem}^2 (the larger the cross-sectional stem area, the lower the resistance to water flow) and h, and is assumed to scale with the size-dependent metabolic rates as: $B \propto Q_0 \propto r_{\text{stem}}^2 \propto M^{3/4} \propto (r_{\text{stem}}^2 h)^{3/4} \propto h^3$. This interconnection in tree geometry is further explained by a series of assumptions such as the fractal-like, self-similar, space-filling and area-preserving branching system (West *et al.*, 2009; Savage *et al.*, 2010). The MST allows mathematical derivation of many plant features, ranging from individual tree spacing to forest biomass density, and provides a potentially powerful foundation for numerous ecological and earth-system modelling attempts (Brown *et al.*, 2004).

The amount of water and energy used for Q_0 given the size of a tree should be balanced with local resource availability (Kempes *et al.*, 2011). Water is a key limiting factor for maximum tree growth (Ryan & Yoder, 1997), and the potential water inflow Q_{p} for the tree is contingent on the absorptance σ_{water} and the accessible water supply I_{water} as: $Q_{\text{p}} \propto \sigma_{\text{water}} I_{\text{water}}$. Energy (light and heat) also constrains maximum tree height (Givnish, 1988). Energy used for metabolism can be translated into the evaporative flow rate Q_{e}, incorporating local solar radiation, air temperature, humidity and wind speed (Sellers *et al.*, 1997). Here, Q_{e} relies on the effective tree area A_{tree} and the evapotranspiration flux E_{flux} derived from the PM equation as: $Q_{\text{e}} \propto A_{\text{tree}} E_{\text{flux}}$.

We are aware of many studies which highlight evidence for deviations from the basic MST and include processes regarding intra-/interspecies variation, plant interaction, self-competition and age-related morphism (Kozlowski & Konarzewski, 2004; Coomes & Allen, 2009; Mori *et al.*, 2010; Piao *et al.*, 2010; Pretzsch & Dieler, 2012; Lin *et al.*, 2013). Nevertheless, it has been generally recognized that species and taxonomic deviations should exist and may also represent predictable evolutionary differences compared with the idealized case (e.g. Brown *et al.*, 2004; Kempes *et al.*, 2011, 2012). This generalization, along with biophysical principles, is still useful for large-scale forest carbon estimations including canopy height mapping, and the derivations of the model do not preclude the incorporation of scaling or process-related differences from the basic MST. Considering the above criticisms and suggestions (Price *et al.*, 2010; Michaletz *et al.*, 2014; Duncanson *et al.*, 2015), we updated the original ASRL research (Kempes *et al.*, 2011; Shi *et al.*, 2013). Although it is still dependent on the quality and quantity of

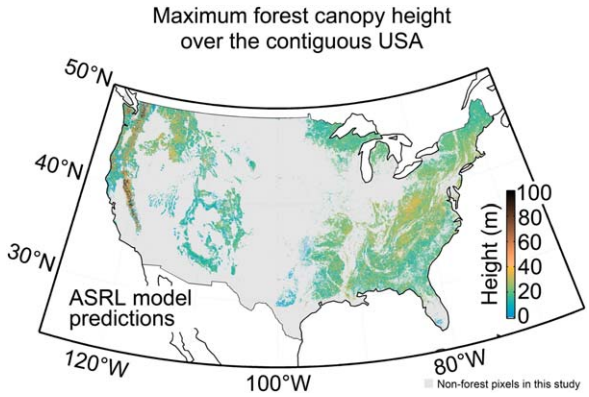

Figure 1 The final allometric scaling and resource limitations (ASRL) model predictions over the contiguous USA. Map of the maximum forest canopy heights over the contiguous USA (*c.* 2005; 1-km^2 grids; Lambert Conformal Conic map projection).

the input data, our approach does have the merit of being prognostic. As a final product, this present study provides a baseline map (*c.* 2005; 1-km^2 spatial resolution) of forest heights over the contiguous United States (Fig. 1). Model evaluation and uncertainty are also discussed.

MATERIALS AND METHODS

The ASRL modelling framework

The ASRL model assumes: (1) a tree should obtain sufficient resources to meet its needs for growth; (2) absorbed light and water (or nutrients) are dependent on tree size; and thus (3) local resource availability limits maximum tree growth (Kempes *et al.*, 2011). In the model this is expressed by inequalities of three flow rates ($Q_p \geq Q_e \geq Q_0$), consisting of the potential rate of water inflow Q_p, the rate of evaporative flow Q_e and the minimum metabolic flow rate Q_0. These flow rates are determined by both tree size and local environmental conditions. Below we describe the basis for and implications of these inequalities. Note that the details on the ASRL model framework and improvements are fully described in Section S1 in the Supporting Information.

The first part of the inequalities is related to local water availability and basal metabolism of trees ($Q_p - Q_0 \geq 0$). A tree must receive enough water to maintain its xylem flow based on a function of tree height h: $Q_0 = \sum^{12\ \text{months}} \beta_1 h^{\eta_1}$, where β_1 and η_1 are the normalization constant and exponent for basal metabolism. The potential water inflow for trees is given as a function of h, elevation and precipitation: $Q_p = \sum^{12\ \text{months}} \gamma(2\pi r_{root}^2)\Psi P_{inc}$. The absorption efficiency γ is related to properties of the local soil and terrain. The hemispheric root surface area $2\pi r_{root}^2$ is derived from the mechanical stability and isometric relationship between the radial root extent r_{root} and h (Niklas, 2007). Elevation is converted into the normalized topographic index Ψ accounting for terrain slope and the direction and accumulation of surface water flow. The long-term monthly precipitation P_{inc} is input to the model as a geospatial predictor.

The potential water inflow and evaporative flow rates are associated with the second part of the inequalities ($Q_p - Q_e \geq 0$). The whole-plant evaporation, $Q_e = a_L v_{water} \sum^{12\ \text{months}} E^{flux}$, should be less than or equal to the water absorption derived from Q_p. Here, Q_e incorporates h, elevation and the other monthly climatic variables, including solar radiation, temperature, vapour pressure and wind speed. The effective tree area a_L accounts for the area of single leaf s_{leaf} and the tree branching architecture (West *et al.*, 1997; Kempes *et al.*, 2011), and v_{water} is the molar volume of water. The PM equation computes the monthly evaporative molar flux E_{flux}. Both a_L and E_{flux} are dependent on tree size.

The last part of the inequality is given as: $Q_e - Q_0 \geq 0$. Size-dependent Q_e is a proxy for metabolic energy use (Sellers *et al.*, 1997). For a given tree size, the life-sustaining water circulation from Q_0 (i.e. the minimum requirement) should not exceed the whole-plant Q_e determining the water–energy balance. On the whole, $Q_p \geq Q_e \geq Q_0$ (Fig. 2). The ASRL model explores the maximum potential h within the boundary where Q_e does not violate the upper (Q_p) and lower (Q_0) limits. The trajectory of all three flow rates varies with local environmental conditions and metabolic scaling relationships.

Key improvements in the ASRL model

Key improvements to the model, which can be grouped into six main categories, are detailed in this section and listed in Table 1. First, the invariant allometric relationship between the height h and the stem radius r_{stem} in the MST model is modified ($h \propto r_{stem}^{\phi}$ with a theoretical $\phi \approx 2/3$). This allows for differences in the scaling exponent θ (metabolic flow rate $Q_0 \propto$ mass M^{θ}) and accounts for variability in metabolic scaling (e.g. Pretzsch & Dieler, 2012; Duncanson *et al.*, 2015). The ecoregional ϕ values were obtained from field-measured h and r_{stem} (see the section 'Data').

Second, the ASRL model in this present study takes into account crown plasticity (Purves *et al.*, 2007) instead of invariant crown geometry. The MST predicts crown height h_{cro} with an isometric relationship: $h_{cro} \approx 0.79\ h$ (Enquist *et al.*, 2009; Kempes *et al.*, 2011). However, this connection is weakened in real forests where open habitat is not common. Trees would have to change their geometry and metabolic scaling features due to interaction between plants (Lin *et al.*, 2013) and self-competition (Smith *et al.*, 2014). We retrieved regional h–h_{cro} allometries from *in situ* data (Data Section).

Third, the improved model estimates the whole-plant energy exchange based on the PM equation. Previous studies aggregated single-leaf energy fluxes (thermal radiation L, sensible heat H and latent heat λE_{flux}) and balanced the sum with the absorbed solar radiation R_{abs}. Instead, the tree crown is treated as a big leaf in our work (Monteith & Unsworth, 2013). The soil heat flux G has also been added to the energy balance: $R_{abs} = L + G + H + \lambda E_{flux}$. Whole-plant heat,

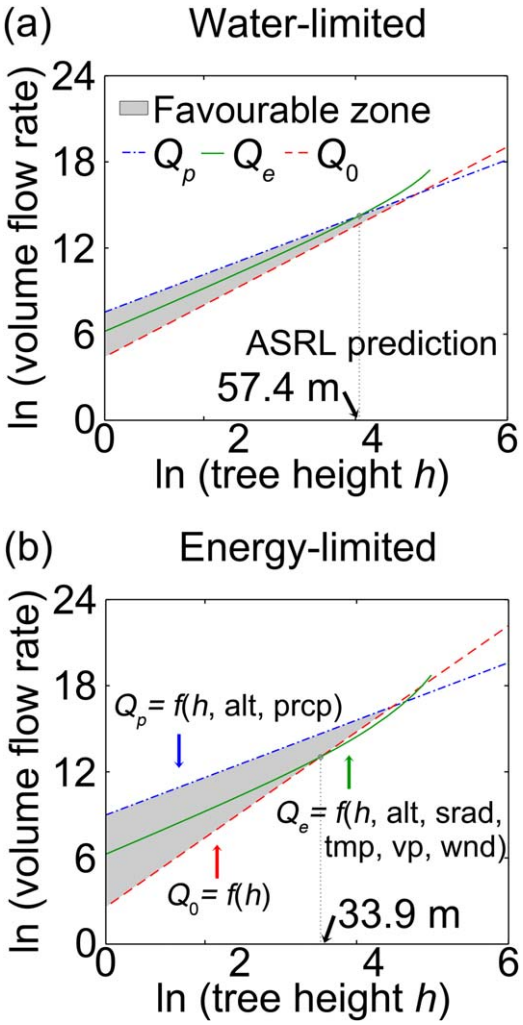

Figure 2 The allometric scaling and resource limitations (ASRL) modelling framework: $Q_p \geq Q_e \geq Q_0$ (Kempes *et al.*, 2011). In the natural logarithm graphs, Q_p is the potential inflow rate (dash-dotted line), Q_e refers to the evaporative flow rate (solid line) and Q_0 corresponds to the basal metabolic flow rate (dashed line). The model predicts the maximum tree height h where Q_e intersects with either Q_p (water limited) or Q_0 (energy limited). Q_e does not violate the upper (Q_p) or lower (Q_0) limits in the favourable zone for trees. The trajectory of all three curves reflects the heterogeneity in local environmental conditions and metabolic scaling relationships. Q_p is a function of tree size (h), altitude (alt) and precipitation (prcp), while Q_e is derived from h, alt, solar radiation (srad), air temperature (tmp), vapour pressure (vp) and wind speed (wnd). Q_0 reflects tree-size-dependent metabolism. Examples of the maximum potential h in the ASRL predictions for (a) a water-limited environment (44.43 °N, 121.72 °W; maximum potential height h_{max} = 57.4 m) and (b) an energy-limited environment (38.41 °N, 80.84 °W; h_{max} = 33.9 m).

aerodynamic and vapour conductances are calculated using local topographic and climatic variables (Allen *et al.*, 1998; see also Section S1.4.3 in the Supporting Information for the detailed formulae).

Fourth, mean annual geospatial predictors are no longer used in the updated model. We used long-term monthly climate data (see 'Data') to compute and accumulate monthly flow rates (Q_p, Q_e and Q_0). Now, the model considers the seasonality in climatic variables, particularly for the evaporative molar flux E_{flux} and so for Q_e. This study also incorporates the growing season (monthly mean air temperature $\geq$ 5 °C) in the estimation of Q_e by assuming that cold temperature alters stomatal opening and water fluidity (Lambers *et al.*, 2008).

Fifth, the normalized topographic index Ψ explicitly reflects local terrain features (e.g. hill, ridge, valley and saddle) in the revised model. From elevation data (see 'Data'), we generated both terrain slope *slp* and specific catchment area *CA* that are further used in the calculation of Ψ (Beven & Kirkby, 1979): $\Psi = \ln[CA/\tan(slp)]/\ln[CA_0/\tan(slp_0)]$ where CA_0 and slp_0 are the normalization slope and catchment area at a flat hilltop. This topographic index supplements the hypothetical water absorption efficiency γ in the preliminary studies (Kempes *et al.*, 2011; Shi *et al.*, 2013).

Lastly, we mitigated the reported discrepancy between modelled and contemporary heights in disturbed forests. The updated ASRL model first predicts the maximum potential heights h_{max} given local resource availability, and then it produces the contemporary heights h_c based on the regional h–age trajectories (a generalized growth curve: $h_c = h_{max}[1 - \exp(-at_c)]^{1/b}$; Richards, 1959; Chapman, 1961). The local metabolic/geometry parameters and geospatial predictors determine the regional h_{max}. Large-scale disturbance history data (see 'Data') provides forest age information t_c for the model. The curvature parameters a and b regulate the inflection point, growth rate and maturation age (Garcia, 1983). Field-measured height h_f and age t_f (Data Section) provide the regional a and b using the above generalized growth curve.

Validation of the model framework, evaluation of results and estimation of uncertainty

The model framework was tested with eddy covariance measurements (FLUXNET; see 'Data') across different ecoregions. We converted the observed latent heat flux λE_{flux} into the evaporative flow rate Q_e (Section S1.4 in Supporting Information) and tested if this FLUXNET Q_e is within the favourable zone (e.g. $Q_p \geq Q_e \geq Q_0$) for trees as previously presented in Fig. 2.

Our final results were evaluated with a variety of reference datasets (see 'Data') including independent field measurements, airborne/spaceborne lidar and existing modelled heights. Model uncertainties at county level were also examined to show the robustness of the ASRL modelled height h_{ASRL}. We estimated local absolute errors relative to the observed heights at each county over the US mainland (% absolute errors).

We additionally included variations in ecoregion and plant functional type in the selected model parameters

Table 1 Key improvements in the ASRL modelling approach compared with the previous studies (Kempes *et al.*, 2011; Shi *et al.*, 2013).

Preliminary studies	Present study
Universal metabolic exponent θ (*c.* 3/4) (metabolic flow rate $Q_0 \propto$ body mass M^{θ})	Varying θ across the contiguous USA based on field observations
Invariant tree crown geometry (tree height h to crown height h_{cro} or to crown radius r_{cro})	Crown plasticity (possible plant interaction and self-competition for light)
Forced up-scaling of single leaf energy balance	Whole-plant energy balance estimation (big leaf)
Long-term mean annual geospatial predictors	Long-term monthly climatic variables with seasonality
Homogeneous local terrain features (flat area)	Topographic index given slope, surface water flow direction and accumulation (e.g. hill, ridge, valley and saddle)
Neglected forest stand age information	Application of large-scale disturbance history data

(normalization constant for the basal metabolism β_1 for the metabolic flow rate Q_0, water absorption efficiency γ for the potential water inflow Q_p and area of a single leaf s_{leaf} for Q_e). The original ASRL model used the bulk quantities of β_1, γ and s_{leaf} based on the literature. This is a way to summarize an entire study region with single parameter values. However, for realistic model applications, those ASRL parameters should not be constant for the whole of the USA. In this study, our parametric adjustment was associated with significant changes in the parameters away from their initial, literature-prescribed values. Kempes *et al.* (2011) tested the sensitivity of bulk parameters and showed the potential for parametric adjustments. The physical meanings of those three parameters and justification for the parametric adjustments are described in Section S1.6 in the Supporting Information and 'Data'.

Data

In situ measurement data were obtained from the Forest Inventory and Analysis study (FIA; Gray *et al.*, 2012) spanning the years from 2003 to 2007. This study incorporated over 2 million valid trees [live and (co-)dominant] to derive the regional allometric scaling relationships (tree height h to stem radius r_{stem} and to crown height h_{cro}). In order to avoid double counting of trees, we used the latest record if a tree was measured more than once. Open grown or overtopped trees defined in the FIA data were excluded in the analyses. Regional stratification of the *in situ* data was made based on 36 provinces (190 sections) of the ecoregion map (Cleland *et al.*, 1997). The maximum height h_f and stand age t_f over the FIA plots were also retrieved. The data were fitted using the robust least-squares regression along with bi-square weights in the MATLAB toolbox (MathWorks, 2014).

For input climate data, including monthly precipitation, solar radiation, air temperature and vapour pressure, we used the DAYMET grids (Thornton *et al.*, 2014) averaged over multiple years from 1981 to 2005. The remaining climate data, on wind speed, were obtained from the long-term monthly National Centers for Environmental Prediction/National Center for Atmospheric Research (NCEP/NCAR) Reanalysis product for the years 1981 to 2010 (Kalnay *et al.*, 1996). Input elevation data were derived from the US Geological Survey (USGS) digital elevation model (Gesch, 2007). For input disturbance history data, we used the North American Carbon Program (NACP) forest stand age grids (*c.* 2006; Pan *et al.*, 2011). All input gridded data were resampled and reprojected to generate the modelled heights at a 1-km spatial resolution with a Lambert Conformal Conic map projection.

Sixty-eight AmeriFlux FLUXNET sites (Barr *et al.*, 2015) were chosen to validate the ASRL model framework. The sites selected were located over the US mainland and active for the years 2001–10 for which the latent heat flux λE_{flux} data ($W m^{-2}$) from the eddy covariance measurement are available for the forest pixels retrieved from the Moderate Resolution Imaging Spectroradiometer (MODIS) land-cover data (Friedl *et al.*, 2010). We first computed long-term monthly averages of λE_{flux}. Our modelled λE_{flux} were then replaced with those FLUXNET measurements in the calculation of evaporative flow rate Q_e calculation: $a_L v_{water} \sum^{12\ months} E_{flux}$. Here, we used the ideal latent heat of evaporation λ (= 44,000 J mol^{-1}) and the molar volume of water v_{water} (= 1.8×10^{-5} m^3 mol^{-1}). The effective tree area a_L was a modelled variable given a local maximum tree size and leaf area (Section S1.4 in the Supporting Information).

Reference height data for the evaluation of model results were derived from multiple *in situ* and airborne and spaceborne lidar campaigns. We used the NACP field measurements (2007–09; Cook *et al.*, 2011; Strahler *et al.*, 2011), Laser Vegetation Imaging Sensor (LVIS) airborne lidar altimetry information from 2003 to 2009 (Blair *et al.*, 2006) and GLAS spaceborne lidar data for 2004–06 (Zwally *et al.*, 2012). Lastly, an existing global forest height product based on a machine learning algorithm (Random Forest) with comparable geopredictors and GLAS-derived heights (Simard *et al.*, 2011) was used for intercomparison of the modelled height estimations.

From each reference dataset, within-pixel heights (1-km^2 grids) were estimated to ensure the validation pairs. For the NACP plots, we used the 90th percentile tree heights for each plot to avoid any outliers related to different sample sizes and measurement errors. The NACP plots were considered valid when 20 or more trees were measured. For LVIS data, the within-footprint maximum metric *RH100* was selected.

We also obtained the 90th percentile of LVIS height h_{LVIS} from about 3000 footprints per pixel. For GLAS data, the waveform extent [from the signal beginning to the first (or second) Gaussian peak] was used to calculate the within-footprint maximum heights. The terrain effect on the large-footprint lidar waveform was corrected (Park *et al.*, 2014). This study excluded low-quality GLAS data with possible low energy returns, signal saturation, cloud contamination and slope gradient effects (Choi *et al.*, 2013; Tang *et al.*, 2014). The ASRL-to-GLAS validation pairs were generated using the 90th percentile of GLAS heights h_{GLAS} from 1 up to 20 footprints per pixel (*c.* 1.51 footprints on average).

The parametric adjustments were performed over 180 subregions based on the 36 ecoprovinces and five forest plant functional types from the MODIS land-cover data. Here it is important to use independent training datasets during the model adjustment process. We thus tested two different training datasets derived from the FIA and GLAS height observations. There were no overlaps within a 10-km radius of each dataset. This study divided the FIA data into two groups where 25% of the data were used for training and we kept the rest (75%) for additional evaluation of the modelled heights. This study also removed training samples within a 10-km radius from the NACP and LVIS measurements to retain the independence of training and evaluation data. Pairing the FIA data and ASRL grids was difficult because FIA plot locations were randomly distorted up to 1.6 km, and about 20% of FIA plots were swapped with ecologically similar plots within the same US county (Guldin *et al.*, 2006). Thus, a 3 km × 3 km moving window was applied to search the FIA data spatially corresponding to the ASRL predictions. We finally obtained 49,075 pairs of ASRL-to-FIA evaluation data, 17,430 pairs of ASRL-to-FIA training data and 34,239 pairs of ASRL-to-GLAS training data.

RESULTS

Validation of the ASRL model framework with FLUXNET data

We found that the values for evaporative flow Q_e calculated from eddy covariance measurements mostly fall within the feasible regime for tree survival described in the model framework (Fig. 3a–d): 90% of FLUXNET data are between the upper (potential water inflow Q_p) and lower (basal metabolic flow Q_0) boundaries of flow rates across multiple regions. Spatial distribution of the FLUXNET sites and four eco-regional groups (A–D) are given in Fig. 3(e). Here, Q_p varies with local water availability and absorption efficiency, and Q_0 reflects the variations in the metabolic scaling and crown geometry parameters that are contingent on the ecoregion and forest plant functional type. The favourable zone for trees slightly disagrees with seven FLUXNET data, mainly associated with evergreen needleleaf forests in Groups A ($n = 1$), B ($n = 3$) and C ($n = 3$). Our FLUXNET calculation of Q_e combines the local maximum forest height with the latent heat exchange averaged over the 0.5–5-km^2 footprint of the eddy flux towers (Baldocchi *et al.*, 2001). These FLUXNET Q_e values could be underestimated due to variation in local tree height. This is not the case of violating the upper boundary Q_p in the model framework and the disparity would be reduced if we applied the local mean height.

Result evaluation

This section provides three case studies of ASRL predictions with (1) no parametric adjustments (Fig. 4a), (2) adjustments using FIA training samples (Fig. 4b), and (3) adjustments using GLAS lidar heights (Fig. 4c). Figure 4(a)–(c) shows scatter plots of the subregional 90th percentile forest heights ($n = 190$ sections of the ecoregion map) from the ASRL predictions, FIA test data, airborne (LVIS)/spaceborne (GLAS) lidar data and Simard's modelled product. For the NACP reference data we present pixel-level comparisons ($n = 51$) instead of the subregional level evaluation because this field campaign was conducted in a few limited regions (three ecosections), mainly in the north-eastern forests.

As shown in Fig. 4(a), case study (1) with the unadjusted ASRL model showed slightly larger disagreements compared with the FIA data [mean absolute error (MAE) = 8.2 m], NACP field measurements (MAE = 7.5 m), GLAS/LVIS lidar altimetry information (MAE = 11.0 m) and Simard's modelled product (MAE = 8.6 m). Our mechanistic model explained only 20–30% of the variations in the *in situ* and lidar heights over the US mainland. Regional Group A (Pacific Northwest, California and Rocky Mountain forests; see Fig. 3e) contributed the largest errors in the modelled heights due to either excessive precipitation (e.g. Pacific Northwest forests) or relatively cold temperature with a short growing season (e.g. Rocky Mountain forests) that the initial parameters could not account for in the ASRL model.

It has been widely noted that field and remote sensing observations can be used to adjust and update theoretical models via initialization or parameterization (Plummer, 2000). Process-based models have bulk parameters, which summarize the rich detail of biophysical principles. One strategy in the model optimization is to match model outputs with actual observations to find the best parameter values that minimize errors. Thus, we conducted the above case studies (2) and (3) with the FIA training data and GLAS lidar data as inputs to the ASRL model, allowing us to modify three critical model parameters (normalization constant β_1 for the basal metabolic flow Q_0, water absorption efficiency γ for the potential water inflow Q_p and area of a single leaf s_{leaf} for the evaporative flow Q_e). In both cases (Fig. 4b,c), the parametric adjustments resulted in a significant improvement in model predictions. We obtained lower MAEs of 4.0 m for case (2) and 5.0 m for case (3) without outliers (Cook's distance; Cook, 1977). Our results also showed better linear relationships with the FIA test data, explaining 64% and 46% of the variations for cases (2) and (3), respectively.

Comparisons between the modelled and NACP heights still retained large MAEs of (2) 7.7 m and (3) 6.5 m. However,

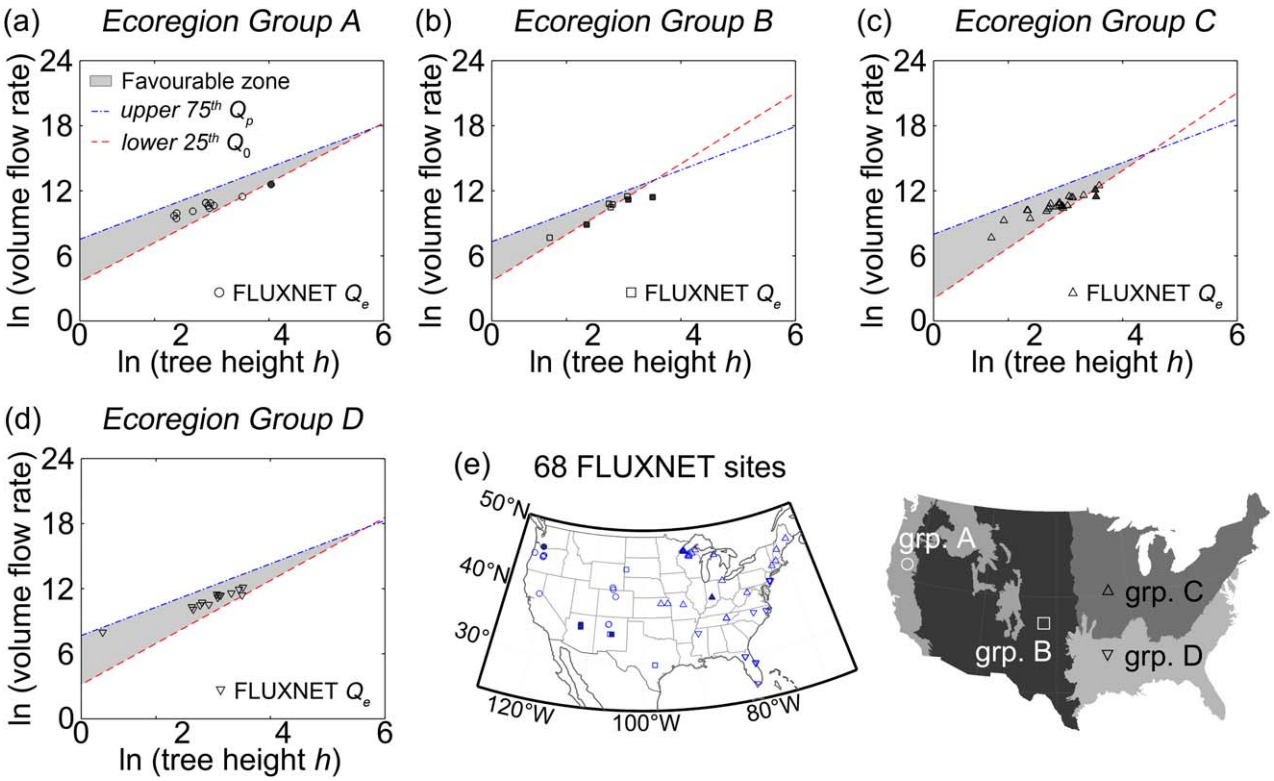

Figure 3 (a)–(d) Validation of the allometric scaling and resource limitations (ASRL) model framework using eddy covariance measurements over four ecoregional groups. Long-term monthly averages of latent heat flux from 68 FLUXNET towers were translated into the evaporative flow Q_e given a local tree size. Annual total precipitation and soil/terrain features determine the potential water inflow rate Q_p, while the basal metabolic flow rate Q_0 reflects the variations with ecoregion and plant functional type. Favourable zones for trees should fulfil the upper boundary Q_p (dash-dotted lines) and the lower boundary Q_0 (dashed lines) where respective lines correspond to the extended (from 25th to 75th percentiles) flow rates for each regional group. (e) Spatial distribution of FLUXNET sites. Ecoregional Groups A (Pacific Northwest, Californian and Rocky Mountain forests), B (Intermountain, south-west semi-desert and Great Plain dry steppe forests), C (North Wood, midwest and north-eastern Appalachian forests), D (south-eastern and outer coastal plain forests). Closed symbols ($n = 7$) represent the FLUXNET sites that exceeded trees' favourable zones in the ASRL model. Table S2 provides more information on the FLUXNET data used in this study.

the majority of comparison pairs from Group C (symbol ×, $n = 43$; north-eastern forests) are located near the 1:1 line, while the NACP data from Group A (symbol *, $n = 8$; southern California forests) showed an underperformance of the ASRL model. Excluding the evaluation pairs from Group A, MAEs were reduced to (2) 4.7 m and (3) 5.2 m. The ASRL model with parametric adjustments was gave better predictions than the unadjusted model, as shown in comparisons with the LVIS and GLAS lidar altimetry data (MAEs of (2) 7.0 m and (3) 6.0 m). Subregional predictions showed better and statistically significant linear relationships with the lidar heights [$R^2 = 0.40$, $y = 0.8x + 2.6$, $P < 0.001$ for case (2); $R^2 = 0.47$, $y = 0.7x + 5.2$, $P < 0.0001$ for case (iii)]. Lastly, we obtained good agreement with the existing modelled heights (Simard's heights) in both case studies [MAE = (2) 4.9 m and (3) 4.2 m] with reasonable linear relationships [$R^2 = 0.58$ and 0.62 for cases (2) and (3), respectively]. Our scatter plots displayed a heavy upper-left tail away from the 1:1 line and large systematic errors [slope = (2) 1.4 and (3) 1.3, intercept = (2) −9.2 and (3) −6.1], but this is because of the absence of large tree samples (> 50 m) in Simard's heights.

Model uncertainty

We calculated absolute errors of the ASRL predictions relative to the FIA test data (% absolute errors = |FIA – ASRL|/FIA × 100) to examine the model uncertainty. From the above three case studies, the 90th percentile heights of the FIA data and model predictions were obtained at US county level. FIA plot locations were distorted and swapped within the same county (see 'Data') and thus, the county-level investigation was the best option for minimizing uncertainties unrelated to the model. Mean values of percentage errors over the US mainland were 34.5%, 16.8% and 19.9% for case studies (1), (2) and (3), respectively. The model parameters were less uncertain over the north-eastern Appalachian, south-eastern and outer coastal plain forests given that the ASRL model performance was generally good and stable (10–15% errors) in all three cases. Our parametric adjustments clearly

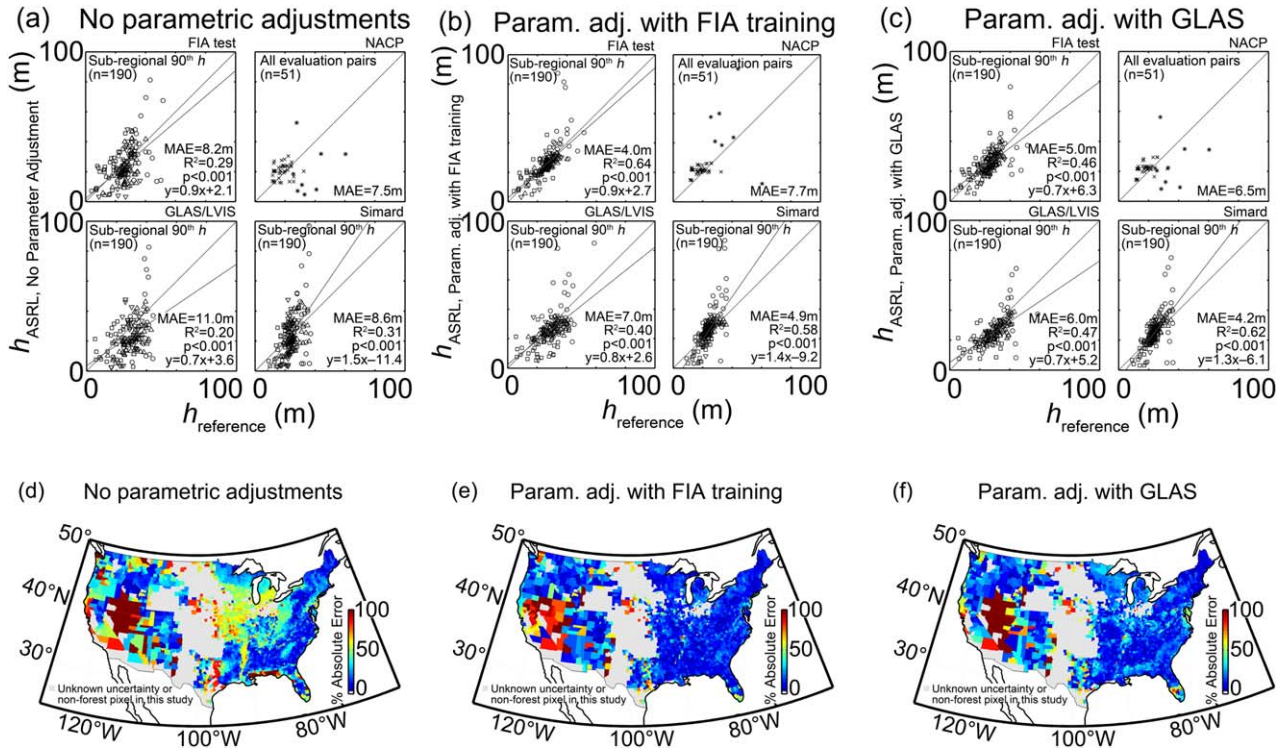

Figure 4 Evaluation of results and model uncertainty. (a)–(c) Allometric scaling and resource limitations (ASRL) predictions of three case studies (1, 2, 3) in comparisons with independent reference datasets: Forest Inventory and Analysis (FIA) test samples, North American Carbon Program (NACP) field measurements, airborne Laser Vegetation Imaging Sensor (LVIS) and spaceborne Geoscience Laser Altimeter System (GLAS) lidar heights, and an existing model product (Simard *et al.*, 2011). Case study (1) represents the model without parameter adjustments, while the other studies (2 and 3) were performed with parametric adjustment using the FIA and GLAS training data. Here, the FIA training samples were spatially independent of the FIA test data (no overlaps within a 10 km radius; see 'Data'). Scatter plots show the subregional 90th percentile forest heights ($n = 190$ sections of the ecoregion map) from ASRL predictions and each reference dataset. For the NACP data, we present pixel-level comparisons ($n = 51$, symbol $\times$ for the north-eastern forests and * for the southern Californian forests) instead of a subregional level evaluation due to under-sampling in a few limited regions. Mean absolute errors (MAE) were calculated without outliers ($> 10\times$ mean of Cook's distance). Linear regressions of the ASRL-to-reference heights are depicted as a solid black line (R^2, slope and intercept are provided). For panels (a)–(c), symbols correspond to four regional Groups A–D. ○, Group A – Pacific Northwest, Californian and Rocky Mountain forests; □, Group B – Intermountain, south-west semi-desert and Great Plain dry steppe forests; △, Group C – North Wood, midwest and north-eastern Appalachian forests; ▽, Group D – south-eastern and outer coastal plain forests. All the regression coefficients are significant (P-value < 0.001). The spatial distribution of reference datasets is given in Fig. S1 in Section S4 of the Supporting Information. (e)–(f) Percentage absolute errors ($= |h_{\mathrm{FIA\ TEST}} - h_{\mathrm{ASRL}}|/h_{\mathrm{FIA\ TEST}} \times 100$) for the model uncertainty. The 90th percentile heights from the FIA data and model predictions using the above three case studies were obtained at US county level to minimize non-model driven uncertainties (i.e. uncertainty in FIA plot location; see 'Data'). Mean values of percentage errors over the US mainland were 34.5%, 16.8% and 19.9% for the three case studies (1, 2, and 3), respectively. Grey represents the US counties with no forest pixels or no FIA test data.

improved the overall predictions, but the quality of the training data may introduce uncertainties in the modelled heights. For instance, case study (2) resulted in errors of about 70% over southern Californian (Sierran coniferous) forests while GLAS training data mitigated those errors in case study (3). A possible reason for this is the relatively large county size with a higher chance of spatial mismatches between the swapped FIA training data and ASRL grids. In future studies it will be important to explore the effect of the accuracy of training data on model predictions. Lastly, we have the lowest confidence in the model over the intermountain semi-desert regions in Groups B, with $> 44.0\%$ errors. Annual precipitation is low in these regions (*c.* 300 mm on average) and the available water inflow Q_p drops below both the evaporative flow Q_e and basal metabolic flow Q_0 without possible corrections as the model parameters exceed their adjustable ranges.

Large-scale pattern of maximum forest canopy heights

The final map of the maximum canopy heights over the contiguous USA is presented in Fig. 1. We used case study (2) with parametric adjustments using the FIA training samples. Table 2 shows the regional averages of model predictions and geopredictors. Overall, the 99th percentile of model heights ${}^{99\mathrm{th}}h_{\mathrm{ASRL}}$ ranged from 28.6 m for Group B to 90.6 m for

Table 2 Eco-regional model predictions and geospatial predictors.

Group	$^{99th}h_{ASRL}$	$^{m}h_{ASRL}$	prcp	srad	tmp	vp	wnd	gdm	age
A	90.6	24.1	1098	348 (0.36)	11.4 (0.33)	564 (0.33)	4.0 (0.17)	6.4	95
B	28.6	12.8	517	396 (0.24)	14.0 (0.37)	601 (0.41)	3.6 (0.11)	7.4	105
C	34.0	21.6	1145	318 (0.29)	14.9 (0.37)	906 (0.58)	4.7 (0.14)	7.5	59
D	39.2	20.0	1377	344 (0.19)	17.7 (0.40)	1467 (0.45)	3.8 (0.15)	11.5	34
Unit	m	m	mm	W m^{-2}	°C	hPa	m s^{-1}	month	year

$^{99th}h_{ASRL}$, the 99th percentile of the modelled maximum forest canopy height h_{ASRL}; $^{m}h_{ASRL}$, mean of h_{ASRL}; prcp, annual total precipitation; srad, mean solar radiation; tmp, mean air temperature; vp, mean vapour pressure; wnd, mean wind speed; gdm, mean growing degree months (monthly mean air temperature ≥ 5 °C); age, mean forest stand age.
For srad, tmp, vp and wnd, we considered the mean values during the gdm. Values in parentheses represent the ecoregional coefficient of variation (standard deviation divided by the mean) to show the seasonality.

Group A. The Pacific Northwest and Californian forest corridors in Group A are predicted to be the most favourable regions for large trees (*c.* 100 m) because of sufficient annual precipitation (> 1400 mm) and moderate mean solar radiation (*c.* 330 W m^{-2}) and air temperature (*c.* 14 °C) during the growing season, where monthly mean temperature is more than or equal to 5 °C. Those are mature forests aged *c.* 100 years on average.

The south-western forests in Group B and the Rocky Mountain forests in Group A are also mature, but exhibit different patterns of maximum canopy height. Annual precipitation is small (500–800 mm) and thus both regions are exposed to lower potential water inflow Q_p compared with the Pacific Northwest/Californian forests. Excessive solar radiation (*c.* 400 W m^{-2}) combined with a relatively high mean temperature (*c.* 16 °C) in the south-western forests produces a large evaporative flow rate Q_e, and the model predicts the lowest h_{ASRL}. On the other hand, the model computes smaller Q_e for the Rocky Mountain forests due to low temperature (*c.* 13 °C) despite similar values for solar radiation. The Rocky Mountain showed the second most favourable environment for large trees (*c.* 50 m).

Medium-sized trees with $^{99th}h_{ASRL}$ of 35–40 m are located over the north-eastern Appalachian forests (Group C) and south-eastern and outer coastal plain forests (Group D), for two reasons. First, moderate temperature during the growing season (15–18 °C on average) generates substantial Q_e, which would compensate for the large water supply available with an annual rainfall of 1200–1400 mm. Second, young forests with recent disturbance have not reached their maximum growth. This is clearly reflected in the predictions, especially for Group D forests aged *c.* 30 years with disturbances such as frequent forest fire and harvest (Pan *et al.*, 2011).

DISCUSSION

Whole-plant energy balance and long-term monthly variables

The long-term averages of the DAYMET and NCEP/NCAR data were useful in the calculation of whole-plant energy balance. We were able to capture the seasonality in the estimation of the evaporative flow rate Q_e where mean annual geospatial predictors did not suffice. For instance, the DAYMET data show similar mean temperature of *c.* 16 °C during the growing season in the Colorado forests and the central Appalachian forests, but their coefficients of variation (CVs; standard deviation divided by mean) are 0.27 and 0.33, respectively. This implies a possible intra-annual variability in the evaporative molar flux E_{flux} and Q_e. Solar radiation over the Californian and south-eastern forests also gives different Q_e, patterns such that the growing season mean is *c.* 350 W m^{-2} while their respective CVs are 0.36 and 0.19. The whole-plant energy balance (the 'big-leaf' approach in this study) still has limitations due to the sunlit and shaded features of leaves (Sprintsin *et al.*, 2012). Nevertheless, our approach was reasonable given the availability of DAYMET data because the 'two-leaf' model requires extra inputs separating direct and diffuse solar radiation.

Implementation of forest age information

The initial predictions of the ASRL model represent the maximum potential height h_{max} on the basis of local resource availability and metabolic scaling (Fig. 5a). However, there are disparities between h_{max} and *in situ* measurements owing to recent disturbances because the theory assumes that all forests are mature. This is shown in the right-skewed histogram of relative errors (median = −3.7 m) in Fig. 5(b). The differences are mainly situated over regional Groups C and D including the North Woods, north-eastern Appalachian and southeast/outer coastal forests. Comparison between the approximated maturation and regional mean forest ages (Fig. 5c) suggests that the majority of regions have not reached their maximum forest growth, except for some unreliable approximations in the intermountain semi-desert forests (Group B). As described in the section 'Model uncertainty', the model was less predictive in the semi-desert regions. Figure 5(d)–(f) displays examples of *h*-stand age trajectories used in the model. Each of the Sierran coniferous forests (Group A), north-eastern mixed forests (Group C) and south-eastern mixed forests (Group D) has three growth curves whose upper asymptote is respectively derived from

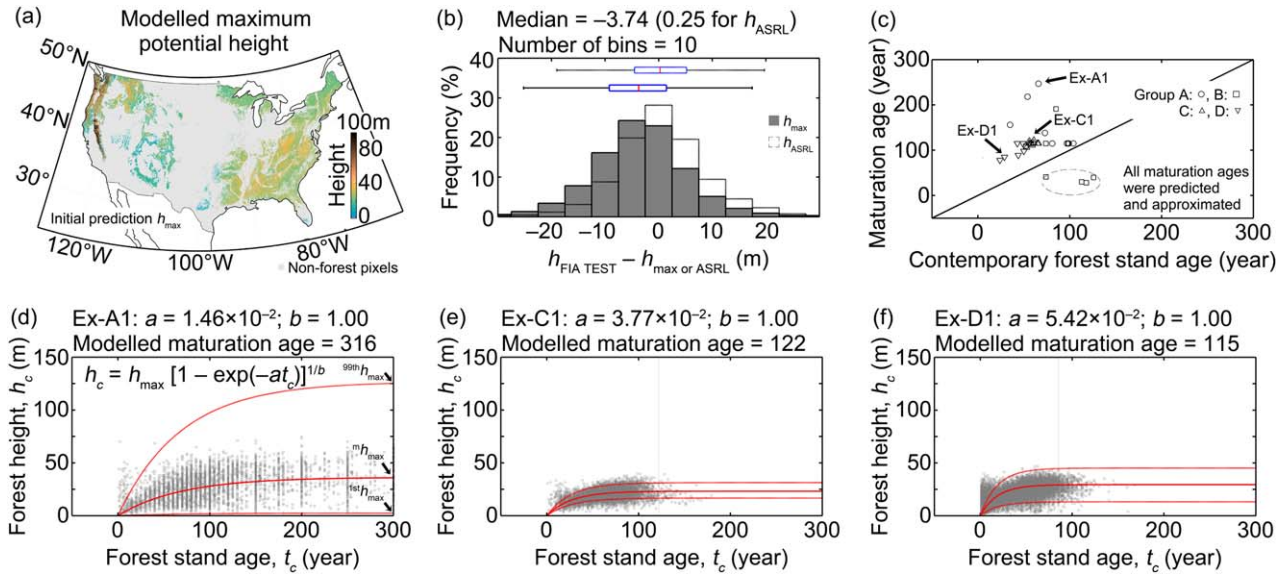

Figure 5 The initial prediction of the allometric scaling and resource limitations (ASRL) model and the implementation of forest age information. (a) The ASRL predictions showing the maximum potential height h_{max}. (b) Right-skewed bar histogram (overestimation) of the errors: $h_{FIA\ TEST} - h_{max}$. There are disparities between h_{max} and $h_{FIA\ TEST}$ [Forest Inventory and Analysis (FIA) data] with recent disturbances. Dashed line histogram and boxplot are associated with h_{ASRL} (median = 0.25 m; Fig. 1). A solid line boxplot over the histogram represents the first and third quartiles (box edges) of the deviations where the median is −3.74 m and whiskers cover 99.3% of data. (c) Comparison between the approximated maturation and the ecoregional mean forest stand ages. The maturation age is predicted from the regional *h*-age trajectories (99% of the sill). The North American Carbon Program (NACP) data provide the contemporary forest ages. Symbols represent regional groups: ○, Group A; □, Group B; △, Group C; ▽, Group D. Our approach may not be suitable for ecoregions in Group B (within the dashed ellipse). The regional *h*–age trajectories for the selected regions Ex-A1 (Sierra coniferous forests), Ex-C1 (north-eastern mixed forests) and Ex-D1 (south-eastern mixed forests) are given in (d)–(f). Regional 99th, 50th and 1st percentile h_{max} determine the upper asymptote for three curves in each region. The curvature parameters *a* and *b* are from the field data. Grey dots correspond to the *in situ* height and age pairs.

the regional 99th, 50th and 1st percentile h_{max} (red lines) values. These trajectories mostly envelop the field-measured forest heights and ages (grey dots). The updated ASRL model first predicts a baseline (maximum state) and then subtracts the disturbance effect based on the above *h*–age relationships.

A highlight of our efforts is that the upper asymptote of the Chapman–Richards' curve is successfully replaced with h_{max}. This maximum potential is comparable to the 'site index' (Ryan & Yoder, 1997) but can be predicted here from the ASRL model given local variations in environment and plant functional type. It is difficult to obtain the site index solely from a regression of field-measured data if the data have not reached the maximum state of the forest, and it may underestimate the upper asymptote of the growth curve. Therefore, our synergistic combination between the ASRL-modelled h_{max} and the field data is a substantial advantage for predicting changes in site quality and age-related productivity.

Sensitivity analysis and prognostic application

In contrast to non-mechanistic approaches, the ASRL model is based on a simple and clear mechanistic understanding of the relationships between forest structure and multiple geo-predictors, including topography and climatic variables. Sensitivity analysis has demonstrated the potential for prognostic applications of the ASRL model (Fig. 6). As shown in Fig. 6(a)–(e), the modelled h_{max} is sensitive to changes in climatic variables, and the direction and magnitude of model sensitivity vary across different regions. For instance, the Pacific Northwest and Californian forest corridors (Group A, symbol ○) are sensitive to both directions of precipitation change and h_{max} decreases with drought, while increasing water availability produces a greater maximum potential height. We find a monomodal sensitivity distribution of h_{max} with temperature. Either warming (> 2 °C) or cooling (< −2 °C) would result in a significant decrease in the potential maximum height ($\Delta h_{max} = -5$ m) over the Pacific Northwest/Californian forests. Changes in vapour pressure and wind speed show similar patterns of monomodal sensitivity. Shifts in h_{max} are least sensitive to solar radiation.

To illustrate how h_{max} changes (Fig. 6f) within the ASRL model, it is useful to consider the example site of Fig. 2(a) (44.43 °N, 121.72 °W) using both precipitation (10% decrease) and temperature (1 °C increase) modifications. Drought would lower the curve of the potential water inflow rate Q_p while warming would lift the curve of the evaporative flow rate Q_e. Thus, in this water-limited environment the

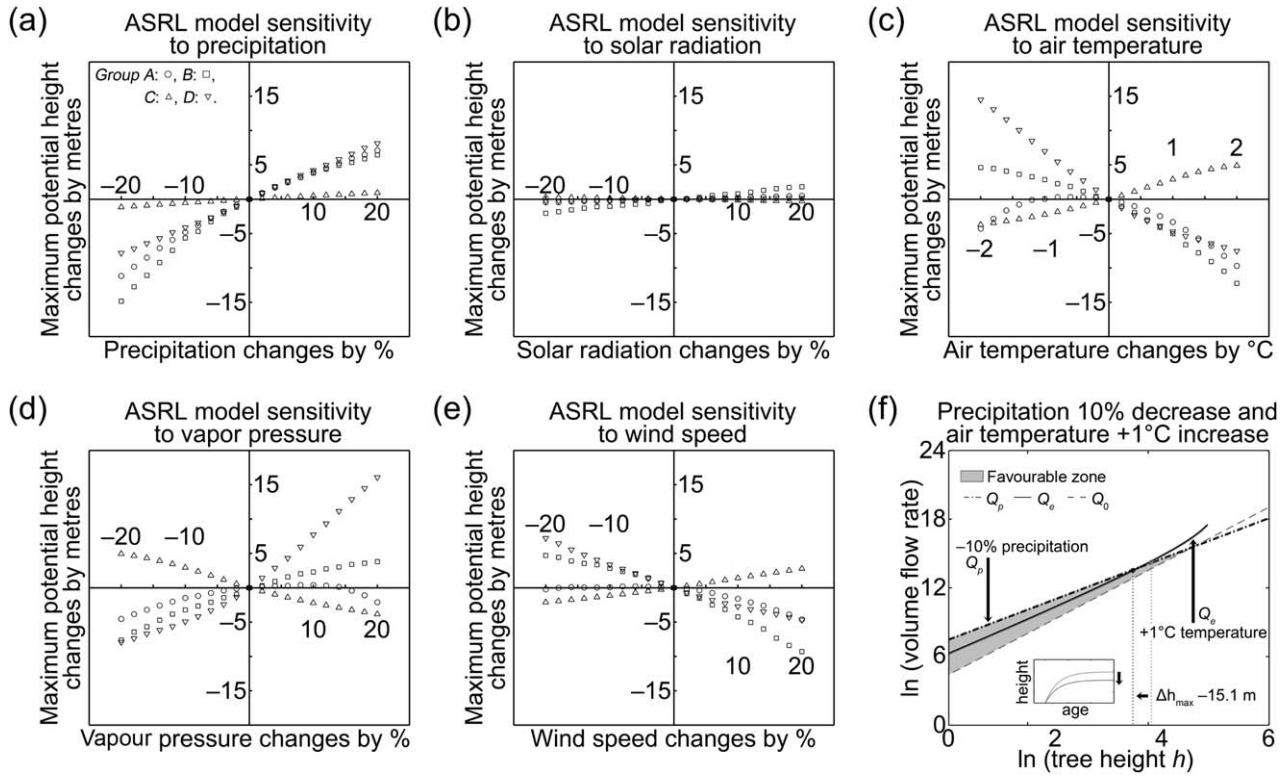

Figure 6 Sensitivity analysis and prognostic application of the allometric scaling and resource limitations (ASRL) model. (a)–(e) The sensitivity of the ASRL model to climatic variables including precipitation, solar radiation, air temperature, vapour pressure and wind speed. Changes in the maximum potential height h_{max} were investigated by perturbing each climatic variable while keeping others constant. Intervals of variable alteration were 0.2 °C for air temperature (ranging from −2 to 2 °C) and 2% for the rest (ranging from −20 to 20%). Mean differences from the no change condition for each regional group (A–D) are displayed: ○, Group A; □, Group B; △, Group C; ▽, Group D. (f) Mechanism for the decrease of h_{max} with both precipitation (10% decrease) and temperature (1 °C increase) modifications (example site from Fig. 2a: 44.43 °N, 121.72 °W; $\Delta h_{max} = -15.1$ m). The drought with reduced precipitation would lower the curve for the potential water inflow rate Q_p while the warming with increased temperature would lift the curve for the evaporative flow rate Q_e. Thus, the intersection between Q_p and Q_e will be shifted to the left (h_{max} decrease) in a water-limited environment. This also implies the degradation of site quality and productivity at a certain forest age shown in the h–age trajectory.

intersection between Q_p and Q_e will be shifted to the left ($\Delta h_{max} = -15.1$ m). This shift is greater than the inherent model errors of ±10 m given the 16.8% overall error in the predicted h_{max} (= 57.4 m) with no changes in climatic variables. In this analysis, the decrease in h_{max} implies the degradation of site quality or productivity at a certain forest stand age as interpreted from the h–age trajectory of Fig. 6(f).

Forest canopy heights predicted from water availability

A recent study (Klein *et al.*, 2015) predicted the maximum forest canopy heights using the difference between precipitation (P), which is an explicit input of our model, and potential evapotranspiration (PET), which is similar to our Q_e. Overall patterns (Fig. 2 of Klein *et al.*, 2015) show good agreement with our final maximum canopy heights, although their methodology was based on a polynomial regression connecting height and water availability (P–PET difference). Figure 2(a) shows the best mechanistic explanation, highlighting the role of water limitation in setting large-scale forest patterns and generating the overall agreement between the ASRL model and the P-PET approach. However, we believe that the low predictability over the boreal forests (Klein *et al.*, 2015) is strongly related to temperature limitation, which can be explained by our mechanism for energy-limited environments (Fig. 2b). The ASRL model and the P-PET approach support each other, and this points towards possible future application of the ASRL model to boreal and tropical forests.

Linking mechanistic models and field and remote sensing measurements

Community efforts in both *in situ* and remote sensing measurements have greatly benefited the capabilities for monitoring forest carbon, but their incomplete data coverage in space and time is still responsible for significant uncertainties in carbon accounting (Le Toan *et al.*, 2011). Also, theoretical and mechanistic models require initialization, adjustment and parameterization using observations to achieve robust predictions of forest carbon (Plummer, 2000). Thus, forest

carbon researchers now have an urgent need for a synergistic combination between mechanistic models and continuous *in situ* and remote sensing measurements at large scales.

This study successfully investigated a mechanistic model in combination with *in situ* and remote sensing measurements to generate large-scale patterns of maximum forest canopy height. Error sources were also examined. In addition, we identified dominant ecological drivers (water and energy) of maximum forest growth and answered how they vary across different ecoregions and forest functional types. The response of forest structure to climate change is one of the most critical elements that is not well incorporated in global carbon monitoring and forecasting.

To conclude, there are two main innovations in this work. First, biophysical principles embedded within the ASRL framework enabled process-based models and actual observations to be combined. We were able to produce large-scale and spatially continuous patterns of forest height while providing a mechanistic understanding of the relationships between forest growth and geopredictors. This procedure has advantages over non-mechanistic models and simple field measurements. The ASRL model alleviated observational discontinuity in space and time. Our strategy in parametric adjustments matched the ASRL predictions with actual measurements and provided the optimal parameter values for minimizing local errors. Meaningful and valid output error specification would be possible using the ASRL model if optimal values of its parameters and input errors are known (e.g. Bayesian analysis). The ASRL framework will be useful in future studies where we can estimate a probabilistic characterization of output errors, which includes the mean and higher-order moments (i.e. bias and uncertainty). Therefore, the ASRL model has the merit of being mechanistic, predictive and robust, whereas prognostic applications and error propagations are difficult for previous models that lacked biophysical principles.

Second, we note that the original ASRL research (Kempes *et al.*, 2011; Shi *et al.*, 2013) has been improved and updated in this paper (Fig. S2 in Section S4 of the Supporting Information). Six key improvements are summarized here: (1) we used varying metabolic scalings across different ecoregions and forest functional types; (2) plant interaction and self-competition were considered; (3) the model calculated whole-plant energy balance; (4) long-term monthly climatic variables were input as geopredictors in order to account for seasonality; (5) topographic features were also included as model inputs; and, most importantly, (6) we took into account the large-scale disturbance histories to reduce the reported discrepancy between potential maximum and contemporary forest heights. This greatly reduces the errors in the original model, which could not account for forest age information and was in essence a steady-state theory. The improved ASRL model can predict both potential upper bound and actual tree sizes given local environmental conditions.

Our research directly responds to major science programmes and missions aiming to quantify, understand and predict global carbon sources/sinks through spaceborne, airborne and field monitoring. Upcoming NASA space missions including ICESat-2 (http://science.nasa.gov/missions/icesat-ii/) and the Global Ecosystem Dynamics Investigation Lidar (GEDI; http://science.nasa.gov/missions/gedi/) will soon enable spatially complete forest height monitoring at the global scale. Therefore, the ASRL model, in a synergistic combination with these missions, will not only facilitate the accurate and continuous forest carbon monitoring but also support carbon forecasting given various climate change scenarios.

ACKNOWLEDGEMENTS

The authors would like to thank the anonymous referees. S.C. was supported by the Fulbright Program for graduate studies, the Bay Area Environmental Research Institute (BAERI) and the NASA Earth and Space Science Fellowship Program (grant NNX13AP55H). S.C. is grateful to NASA Earth Exchange (NEX) for providing the opportunity to access all the data needed for the project and model runs using their computational resources. C.P.K. acknowledges the Omidyar Fellowship at The Santa Fe Institute.

REFERENCES

Allen, R.G., Pereira, L.S., Raes, D. & Smith, M. (1998) Crop evapotranspiration: guidelines for computing crop water requirements. *FAO irrigation and drainage paper* **56**. Food and Agriculture Organization of the United Nations, Rome.

Baldocchi, D., Falge, E., Gu, L.H. *et al.* (2001) FLUXNET: a new tool to study the temporal and spatial variability of ecosystem-scale carbon dioxide, water vapor, and energy flux densities. *Bulletin of the American Meteorological Society*, **82**, 2415–2434.

Barr, J.G., Bible, K., Blanken, P. *et al.* (2015) FLUXNET data from the US-Bar, US-Blk, US-Blo, US-CaV, US-Ced, US-ChR, US-CPk, US-Dix, US-Dk1, US-Dk2, US-Dk3, US-Fmf, US-FR2, US-FR3, US-Fuf, US-Fwf, US-GLE, US-GMF, US-Goo, US-Ha1, US-Ha2, US-Ho1, US-Ho2, US-Ho3, US-KFS, US-Kon, US-KS1, US-KS2, US-Los, US-Me1, US-Me2, US-Me3, US-Me5, US-Me6, US-MMS, US-MOz, US-Mpj, US-MRf, US-NC1, US-NC2, US-NMj, US-NR1, US-Oho, US-PFa, US-Skr, US-Slt, US-SP1, US-SP2, US-SP3, US-Syv, US-UMB, US-UMd, US-Vcm, US-Vcp, US-WBW, US-WCr, US-Wi0, US-Wi1, US-Wi2, Us-Wi3, US-Wi4, US-Wi5, US-Wi6, US-Wi7, US-Wi8, US-Wi9, US-Wjs, US-Wrc. Oak Ridge National Laboratory Distributed Active Archive Center, Oak Ridge, TN. Available at: http://fluxnet.ornl.gov (accessed 1 June 2015).

Beven, K.J. & Kirkby, M.J. (1979) A physically based, variable contributing area model of basin hydrology. *Hydrological Sciences Bulletin*, **24**, 43–69.

Blair, B., Hofton, M.A. & Rabine, D.L. (2006) *NASA LVIS elevation and canopy (LGE, LCE and LGW) data products.*

NASA Goddard Space Flight Center, Greenbelt, MD. Available at: http://lvis.gsfc.nasa.gov (accessed on 15 October 2014).

Brown, J.H., Gillooly, J.F., Allen, A.P., Savage, V.M. & West, G.B. (2004) Toward a metabolic theory of ecology. *Ecology*, **85**, 1771–1789.

Chapman, D.G. (1961) Statistical problems in dynamics of exploited fisheries populations. *Proceedings of the Fourth Berkeley Symposium on Mathematical Statistics and Probability, vol. 4: contributions to biology and problems of medicine*, (ed. by J. Neyman) pp. 153–168. University of California Press, Berkeley, CA.

Choi, S., Ni, X., Shi, Y., Ganguly, S., Zhang, G., Duong, H., Lefsky, M., Simard, M., Saatchi, S., Lee, S., Ni-Meister, W., Piao, S., Cao, C., Nemani, R. & Myneni, R. (2013) Allometric scaling and resource limitations model of tree heights: part 2. Site based testing of the model. *Remote Sensing*, **5**, 202–223.

Cleland, D.T., Avers, P.E., Mcnab, W.H., Jensen, M.E., Bailey, R.G., King, T. & Russell, W.E. (1997) *National hierarchical framework of ecological units*, pp. 181–200. Yale University Press, New Haven, CT.

Cook, B., Dubayah, R., Hall, F., Nelson, R., Ranson, J., Strahler, A., Siqueira, P., Simard, M. & Griffith, P. (2011) *NACP New England and Sierra National Forests biophysical measurements: 2008–2010*. Oak Ridge National Laboratory Distributed Active Archive Center, Oak Ridge, TN. Available at: http://daac.ornl.gov (accessed 15 October 2014).

Cook, R.D. (1977) Detection of influential observation in linear-regression. *Technometrics*, **19**, 15–18.

Coomes, D.A. & Allen, R.B. (2009) Testing the metabolic scaling theory of tree growth. *Journal of Ecology*, **97**, 1369–1373.

Duncanson, L.I., Dubayah, R.O. & Enquist, B.J. (2015) Assessing the general patterns of forest structure: quantifying tree and forest allometric scaling relationships in the United States. *Global Ecology and Biogeography*, **24**, 1465–1475.

Enquist, B.J., West, G.B. & Brown, J.H. (2009) Extensions and evaluations of a general quantitative theory of forest structure and dynamics. *Proceedings of the National Academy of Sciences USA*, **106**, 7046–7051.

Friedl, M.A., Sulla-Menashe, D., Tan, B., Schneider, A., Ramankutty, N., Sibley, A. & Huang, X.M. (2010) MODIS collection 5 global land cover: algorithm refinements and characterization of new datasets. *Remote Sensing of Environment*, **114**, 168–182.

Garcia, O. (1983) A stochastic differential equation model for the height growth of forest stands. *Biometrics*, **39**, 1059–1072.

Gesch, D.B. (2007) The national elevation dataset. *Digital elevation model technologies and applications: the DEM user's manual* (ed. by D. Maune), pp. 99–118. American Society for Photogrammetry and Remote Sensing, Bethesda, MD.

Givnish, T.J. (1988) Adaptation to sun and shade – a whole-plant perspective. *Australian Journal of Plant Physiology*, **15**, 63–92.

Goetz, S. & Dubayah, R. (2011) Advances in remote sensing technology and implications for measuring and monitoring forest carbon stocks and change. *Carbon Management*, **2**, 231–244.

Goetz, S., Baccini, A., Laporte, N., Johns, T., Walker, W., Kellndorfer, J., Houghton, R. & Sun, M. (2009) Mapping and monitoring carbon stocks with satellite observations: a comparison of methods. *Carbon Balance and Management*, **4**, 2.

Gray, A.N., Brandeis, T.J., Shaw, J.D., McWilliams, W.H., Miles, P.D. (2012) Forest inventory and analysis database of the United States of America (FIA). Vegetation databases for the 21st century (ed. by J. Dengler, J. Oldeland, F. Jansen, M. Chytry, J. Ewald, M. Finckh, F. Glockler, G. Lopez-Gonzalez, R.K. Peet, J.H.J. Schaminee), *Biodiversity and Ecology*, **4**, 225–231.

Guldin, R.W., King, S.L. & Scott, C.T. (2006) Vision for the future of FIA: paean to progress, possibilities, and partners. *Proceedings of the Sixth Annual Forest Inventory and Analysis Symposium* (ed. by R.E. McRoberts, G.A. Reams, P.C. Van Duesen, W.H. McWilliams), pp. 1–8. Gen. Tech. Rep. WO-70. US Department of Agriculture Forest Service, Washington, DC.

Hansen, A.J., Phillips, L.B., Dubayah, R., Goetz, S. & Hofton, M. (2014) Regional-scale application of lidar: variation in forest canopy structure across the southeastern US. *Forest Ecology and Management*, **329**, 214–226.

Kalnay, E., Kanamitsu, M., Kistler, R. *et al.* (1996) The NCEP/NCAR 40-year reanalysis project. *Bulletin of the American Meteorological Society*, **77**, 437–471.

Kempes, C.P., West, G.B., Crowell, K. & Girvan, M. (2011) Predicting maximum tree heights and other traits from allometric scaling and resource limitations. *PLoS One*, **6**. e20551, doi:10.1371/journal.pone.0020551.

Kempes, C.P., Dutkiewicz, S. & Follows, M.J. (2012) Growth, metabolic partitioning, and the size of microorganisms. *Proceedings of the National Academy of Sciences USA*, **109**, 495–500.

Kleiber, M. (1947) Body size and metabolic rate. *Physiological Reviews*, **27**, 511–541.

Klein, T., Randin, C. & Korner, C. (2015) Water availability predicts forest canopy height at the global scale. *Ecology Letters*, **18**, 1311–1320.

Kozlowski, J. & Konarzewski, M. (2004) Is West, Brown and Enquist's model of allometric scaling mathematically correct and biologically relevant? *Functional Ecology*, **18**, 283–289.

Lambers, H., Chapin, F.S. & Pons, T.L. (2008) *Plant physiological ecology*, pp. 163–217. Springer, New York.

Le Toan, T., Quegan, S., Davidson, M.W.J., Balzter, H., Paillou, P., Papathanassiou, K., Plummer, S., Rocca, F., Saatchi, S., Shugart, H. & Ulander, L. (2011) The BIOMASS mission: mapping global forest biomass to better

understand the terrestrial carbon cycle. *Remote Sensing of Environment*, **115**, 2850–2860.

Lefsky, M.A. (2010) A global forest canopy height map from the Moderate Resolution Imaging Spectroradiometer and the Geoscience Laser Altimeter System. *Geophysical Research Letters*, **37**, L15401.

Lin, Y., Berger, U., Grimm, V., Huth, F. & Weiner, J. (2013) Plant interactions alter the predictions of metabolic scaling theory. *PLoS One*, **8**, doi:10.1371/journal.pone.0057612.

Mathworks (2014) *Statistics and machine learning toolbox user's guide*, pp. **9**:1–9:187. The Mathworks Inc., Natick, MA.

Michaletz, S.T., Cheng, D.L., Kerkhoff, A.J. & Enquist, B.J. (2014) Convergence of terrestrial plant production across global climate gradients. *Nature*, **512**, 39–43.

Monteith, J. & Unsworth, M. (2013) *Principles of environmental physics: plants, animals, and the atmosphere, 4th edn*, pp. 217–247. Academic Press, Oxford.

Mori, S., Yamaji, K., Ishida, A. *et al.* (2010) Mixed-power scaling of whole-plant respiration from seedlings to giant trees. *Proceedings of the National Academy of Sciences USA*, **107**, 1447–1451.

Nemani, R.R., Keeling, C.D., Hashimoto, H., Jolly, W.M., Piper, S.C., Tucker, C.J., Myneni, R.B. & Running, S.W. (2003) Climate-driven increases in global terrestrial net primary production from 1982 to 1999. *Science*, **300**, 1560–1563.

Niklas, K.J. (2007) Maximum plant height and the biophysical factors that limit it. *Tree Physiology*, **27**, 433–440.

Pan, Y., Chen, J.M., Birdsey, R., McCullough, K., He, L. & Deng, F. (2011) Age structure and disturbance legacy of North American forests. *Biogeosciences*, **8**, 715–732.

Pan, Y., Birdsey, R.A., Phillips, O.L. & Jackson, R.B. (2013) The structure, distribution, and biomass of the world's forests. *Annual Review of Ecology, Evolution, and Systematics*, **44**, 593–622.

Park, T., Kennedy, R.E., Choi, S., Wu, J.W., Lefsky, M.A., Bi, J., Mantooth, J.A., Myneni, R.B. & Knyazikhin, Y. (2014) Application of physically-based slope correction for maximum forest canopy height estimation using waveform lidar across different footprint sizes and locations: tests on LVIS and GLAS. *Remote Sensing*, **6**, 6566–6586.

Peng, S.S., Piao, S.L., Ciais, P., Myneni, R.B., Chen, A.P., Chevallier, F., Dolman, A.J., Janssens, I.A., Penuelas, J., Zhang, G.X., Vicca, S., Wan, S.Q., Wang, S.P. & Zeng, H. (2013) Asymmetric effects of daytime and night-time warming on Northern Hemisphere vegetation. *Nature*, **501**, 88–92.

Piao, S.L., Luyssaert, S., Ciais, P., Janssens, I.A., Chen, A.P., Cao, C., Fang, J.Y., Friedlingstein, P., Luo, Y.Q. & Wang, S.P. (2010) Forest annual carbon cost: a global-scale analysis of autotrophic respiration. *Ecology*, **91**, 652–661.

Plummer, S.E. (2000) Perspectives on combining ecological process models and remotely sensed data. *Ecological Modelling*, **129**, 169–186.

Pretzsch, H. & Dieler, J. (2012) Evidence of variant intra- and interspecific scaling of tree crown structure and relevance for allometric theory. *Oecologia*, **169**, 637–649.

Price, C.A., Gilooly, J.F., Allen, A.P., Weitz, J.S. & Niklas, K.J. (2010) The metabolic theory of ecology: prospects and challenges for plant biology. *New Phytologist*, **188**, 696–710.

Purves, D.W., Lichstein, J.W. & Pacala, S.W. (2007) Crown plasticity and competition for canopy space: a new spatially implicit model parameterized for 250 North American tree species. *PLoS One*, **2, e**870. doi:10.1371/journal.pone.0000870.

Richards, F.J. (1959) A flexible growth function for empirical use. *Journal of Experimental Botany*, **10**, 290–301.

Ryan, M.G. & Yoder, B.J. (1997) Hydraulic limits to tree height and tree growth. *Bioscience*, **47**, 235–242.

Savage, V.M., Bentley, L.P., Enquist, B.J., Sperry, J.S., Smith, D.D., Reich, P.B. & von Allmen, E.I. (2010) Hydraulic trade-offs and space filling enable better predictions of vascular structure and function in plants. *Proceedings of the National Academy of Sciences USA*, **107**, 22722–22727.

Sellers, P.J., Dickinson, R.E., Randall, D.A., Betts, A.K., Hall, F.G., Berry, J.A., Collatz, G.J., Denning, A.S., Mooney, H.A., Nobre, C.A., Sato, N., Field, C.B. & Henderson-Sellers, A. (1997) Modeling the exchanges of energy, water, and carbon between continents and the atmosphere. *Science*, **275**, 502–509.

Shi, Y., Choi, S., Ni, X., Ganguly, S., Zhang, G., Duong, H., Lefsky, M., Simard, M., Saatchi, S., Lee, S., Ni-Meister, W., Piao, S., Cao, C., Nemani, R. & Myneni, R. (2013) Allometric scaling and resource limitations model of tree heights: part 1. Model optimization and testing over continental USA. *Remote Sensing*, **5**, 284–306.

Simard, M., Pinto, N., Fisher, J.B. & Baccini, A. (2011) Mapping forest canopy height globally with spaceborne lidar. *Journal of Geophysical Research–Biogeosciences*, **116**, G04021. doi:10.1029/2011jg001708.

Smith, D.D., Sperry, J.S., Enquist, B.J., Savage, V.M., McCulloh, K.A. & Bentley, L.P. (2014) Deviation from symmetrically self-similar branching in trees predicts altered hydraulics, mechanics, light interception and metabolic scaling. *New Phytologist*, **201**, 217–229.

Sprintsin, M., Chen, J.M., Desai, A. & Gough, C.M. (2012) Evaluation of leaf-to-canopy upscaling methodologies against carbon flux data in North America. *Journal of Geophysical Research–Biogeosciences*, **117**, G01023, doi:10.1029/2010jg001407.

Stojanova, D., Panov, P., Gjorgjioski, V., Kohler, A. & Dzeroski, S. (2010) Estimating vegetation height and canopy cover from remotely sensed data with machine learning. *Ecological Informatics*, **5**, 256–266.

Strahler, A.H., Schaaf, C., Woodcock, C., Jupp, D., Culvenor, D., Newnham, G., Dubayah, R., Yao, T., Zhao, F. & Yang, X. (2011) *ECHIDNA Lidar campaigns: forest canopy*

imagery and field data, U.S.A., 2007–2009. Oak Ridge National Laboratory Distributed Active Archive Center, Oak Ridge, TN. Available at: http://daac.ornl.gov (accessed 15 October 2014).

Tang, H., Dubayah, R., Brolly, M., Ganguly, S. & Zhang, G. (2014) Large-scale retrieval of leaf area index and vertical foliage profile from the spaceborne waveform lidar (GLAS/ICESat). *Remote Sensing of Environment*, **154**, 8–18.

Thornton, P.E., Thornton, M.M., Mayer, B.W., Wilhelmi, N., Wei, Y., Devarakonda, R. & Cook, R.B. (2014) *Daymet: daily surface weather data on a 1-km grid for North America*. Oak Ridge National Laboratory Distributed Active Archive Center, Oak Ridge, TN. Available at: http://daac.ornl.gov (accessed on 15 October 2014).

West, G.B., Brown, J.H. & Enquist, B.J. (1997) A general model for the origin of allometric scaling laws in biology. *Science*, **276**, 122–126.

West, G.B., Brown, J.H. & Enquist, B.J. (1999) A general model for the structure and allometry of plant vascular systems. *Nature*, **400**, 664–667.

West, G.B., Enquist, B.J. & Brown, J.H. (2009) A general quantitative theory of forest structure and dynamics. *Proceedings of the National Academy of Sciences USA*, **106**, 7040–7045.

Wu, Z.T., Dijkstra, P., Koch, G.W., Penuelas, J. & Hungate, B.A. (2011) Responses of terrestrial ecosystems to temperature and precipitation change: a meta-analysis of experimental manipulation. *Global Change Biology*, **17**, 927–942.

Zwally, H.J., Schutz, R., Bentley, C., Bufton, J., Herring, T., Minster, J., Spinhirne, J. & Thomas, R. (2012) *GLAS/ICEsat L2 global land surface altimetry data*, Version 33. NASA DAAC at the National Snow and Ice Data Center, Boulder, CO. Available at: http://nsidc.org/data/GLAH14 (accessed 15 October 2014).

SUPPORTING INFORMATION

Additional Supporting Information may be found in the online version of this article.

Section S0 Acronyms, symbols and abbreviations used in this study.
Section S1 ASRL model framework.
Section S2 References for Supporting Information.
Section S3 Supporting tables.
Section S4 Supporting figures.
Section S5 Sample code for ASRL model (MATLAB).

BIOSKETCH

Sungho Choi is interested in monitoring and modelling forest ecosystem dynamics across spatial and temporal scales. He currently works on the application of the metabolic scaling theory and water–energy balance equation to predict the large-scale patterns of forest canopy height and aboveground biomass.

Editor: Brian McGill